Automatic Microaneurysm Detection and Characterization Through Digital Color Fundus Images*

C.I.O. Martins[1], R.M.S.Veras[1], G.L.B.Ramalho[2], F.N.S.Medeiros[1], D. M. Ushizima[3]
[1]Vision, Images and Signals Laboratory
Universidade Federal do Ceará - Brazil
[2]Centro Federal de Educação Tecnológica do Ceará - Brazil
[3]Math and Visualization Groups
Lawrence Berkeley National Laboratory - USA
{charlesiury,danicyber}@gmail.com,{rveras,fsombra}@ufc.br,gramalho@cefetce.br

Abstract

Ocular fundus images can provide information about retinal, ophthalmic, and even systemic diseases such as diabetes. Microaneurysms (MAs) are the earliest sign of Diabetic Retinopathy, a frequently observed complication in both type 1 and type 2 diabetes. Robust detection of MAs in digital color fundus images is critical in the development of automated screening systems for this kind of disease. Automatic grading of these images is being considered by health boards so that the human grading task is reduced. In this paper we describe segmentation and the feature extraction methods for candidate MAs detection. We show that the candidate MAs detected with the methodology have been successfully classified by a MLP neural network (correct classification of 84%*).*

1. Introduction

Diabetic Retinopathy (DR) is a frequently observed complication in both type 1 and type 2 diabetes, specially in patients with long term disease and poor glycemic control. Irreversible visual loss appears at the final stages of DR and it is considered one of the most tragic of diabetic complications. It is also considered an important factor of morbidity and has a high economical impact once it is the leading cause of blindness in the working population [15]. The pathophysiology of the retinal microvascular alterations is related to the chronic hyperglycemia that leads to the following circulatory disturbances: loss of vascular tonus, increase in vascular permeability, edema and exudation, with vascular obstruction and ischemia that stimulates neovascularization [1]. DR is a major cause of adult blindness due to changes in blood vessels structure and distribution such as new vessel growth (proliferative diabetic retinopathy) and requires laborious analysis from specialist [21].

DR produces a variety of lesions on the retina. MAs are likely to be the only lesion present at the earliest stage of the disease and continue to be present as the disease develops. Thus, the early knowledge and study of these lesions on the retina has a major importance to develop automated retinopathy detection systems. MAs are swellings of the capillaries caused by a weakening of the vessel wall. In retinal photographs, although the capillaries are not visible, MAs appear as dark red isolated dots. In common with vessels, microaneurysms appear with highest contrast in the green-plane of the color image [9, 17]. In normal retinas, dots are also present in image as low contrast pixels compared to MAs. The basic characteristics of MAs are a fairly uniform shape and having a limited range of size, which leads to the use of basic morphology for the identification of candidate MAs [23].

Ocular fundus image can provide information about the pathological changes caused by local ocular diseases. Analyzing and interpreting fundus images have become a necessary and important diagnostic procedure in ophthalmology. Medical image analysis is a research area that is currently attracting multi-disciplinary scientists and physicians. This field involves the study of digital images with the objective of providing computational tools which will assist the quantification and visualization of interesting pathologies and anatomical structures. The progress achieved in this field over recent years has significantly improved the type of medical care that is available to patients.

The retina is the only location where blood vessels can be directly visualized non-invasively in vivo. Increasing technology leading to the development of digital imaging systems over the past two decades has revolutionized fundal

*This work was supported by the U.S. Department of Energy under Contract No. DE-AC02-05CH11231.

imaging [16]. Automated analysis of retinal images has the potential to reduce the screening program costs compared to manual image grading [4].

In this paper we have developed a prototype system for candidate MAs detection in color fundus images. The proposed approach is a modified version of the algorithm presented in [5, 23] and it consists of two main steps. The first one detects candidate MAs (Sections 2.1, 2.2, 2.3) and the second one classifies these candidates as MAs or not using a MLP neural network (Sections 2.4, 2.5).

Artificial neural network (ANN), more often simply called "neural networks", are nonparametric pattern recognition techniques that can recognize "hidden patterns" between independent and dependent variables [8]. Neural networks have been used in a number of applications such as remote sensing [6], medicine diagnosis [10], and pattern classification [13, 18]. Neural network results have been commonly achieved relative to standard statistical models. In this work we utilize the ability of neural network to recognize complex and nonlinear relationship in characterizing candidate MAs.

This paper is organized as follows. Section 2 describes the steps of a general system for MAs detection, including the candidate MAs segmentation, features extraction and classification. Section 3 relates the experimental results using neural networks to classify MAs in retina. Finally, Section 4 briefly outlines our conclusion and future work.

2. Candidate Microaneurysms Segmentation

A general methodology for candidate MAs segmentation is summarized in Figure 1. It was originally proposed by Spencer *et al.* [23] and Frame *et al.*[5] and was used by several authors to detect candidate MAs [12, 14, 20, 25]. In our paper the step concerning candidate MAs extraction is accomplished using the algorithm proposed in [15]. It was originally proposed to detect red lesions in digital color fundus image and we have adapted it for microaneurysms detection.

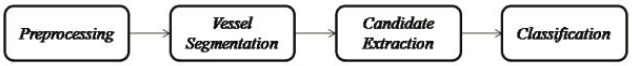

Figure 1. Candidate MAs detection scheme.

2.1. Image preprocessing

The preprocessing module in Figure 1 provides an uniform fundus image for candidates extraction. The image preprocessing is performed on the green chanel I_{green} of the original RGB image I_{org}. As red lesions present the highest contrast with the background in the green color plane [9, 17], information from the red and blue color planes are discarded.

Digital images often contain intensity variations in the background. This effect usually degrades the performance of the system to select candidates. Small intensity variations in the green-plane image background, I_{green}, are removed in the preprocessing step resulting in a "shade corrected" image, I_{sc}.

This shade correction is accomplished by subtracting the background I_{bg} image from the I_{green} image. The background image, I_{bg}, is estimated by smoothing the I_{green} image with a median filter of 25 x 25 pixels size.

$$I_{sc} = I_{green} - I_{bg} \tag{1}$$

2.2. Vessel Segmentation

The vessel segmentation module in Figure 1 refers to the process of finding the vasculature map I_{vas} and subtract it from the image I_{sc}. Previous papers [14, 20, 25, 12] achieved vessel segmentation by applying a morphological opening to the shade-corrected image using a long linear single pixel wide structuring element at various orientations. These openings are combined by choosing the maximal response at each pixel out of all the openings and then subtracting the result from the shade-corrected image. This image difference so-called top-hat transformation extracts details which may correspond to MAs. Furthermore, these morphological operators do not distinguish between MA and elongated structures, requiring another step to solve this problem.

In this paper we have used for this purpose the algorithm proposed in [26], which is a general vessel segmentation method based on mathematical morphology and curvature evaluation. The authors assume that the vascular tree is the only element of the retinal image that is locally uniform in color or gray value completely described by the following properties:

1. the shape of a cross-section looks like a Gaussian curve;
2. it is connected in a tree-like way;
3. vessels have a certain width and cannot be too close together.

These properties can be separated into those related to the morphological description (e.g. linearity, connectivity, vessel width) and those related to the calculation of some parameters (e.g. the curve of the Gaussian profile, its variation along the crest lines). There are different kinds of undesirable patterns encountered when extracting the vascular tree, including candidate MAs.

The algorithm proposed for digital retinal angiography and for green images of the eyes fundus [26] consisted of several morphological operations, using a set of linear structuring elements L_i (every $15°$) with 15-pixels long and 1-pixel wide, summarized as follows:

$$S_{op} = \gamma^{rec}_{I_{sc}}(\mathrm{Max}_{i=1...12}\{\gamma_{L_i}(I_{sc})\}), \quad (2)$$

$$S_{sum} = \sum_{i=1}^{12}(S_{op} - \gamma_{L_i}(I_{sc})). \quad (3)$$

Eq. (2) performs a linear opening by reconstruction with an element of size 15 on image I_{sc}. This operation removes every isolated round and bright zones whose diameter is less than 15 pixels, resulting in the image S_{op}. Eq. (3) performs a sum of top hats to reduce small bright noise and to improve the contrast of all linear parts within S_{op}, leading to the image S_{sum}.

Vessels could be manually segmented by using a simple threshold on S_{sum}. However, these images are noisy and require further treatment. Zana *et. al* [26] have proven that the sign of the Laplacian filter applied to image S_{sum} can be used as a good approximation of the curvature sign [3]. According to Eq. (4) this sign can be observed in image S_{lap} where a Gaussian smoothing is performed on image S_{sum}. The computation of the curvature is completed with the Laplacian operation.

$$S_{lap} = Laplacian(Gaussian^{width=7\mathrm{px}}_{\sigma=7/4}(S_{sum})) \quad (4)$$

Finally, the image I_{vas} is obtained according to the alternating filter described in [22] and showed in the following:

$$S_1 = \gamma^{rec}_{S_{lap}}(\mathrm{Max}_{i=1...12}\{\gamma_{L_i}(S_{lap})\}), \quad (5)$$

$$S_2 = \phi^{rec}_{S_1}(\mathrm{Min}_{i=1...12}\{\phi_{L_i}(S_1)\}), \quad (6)$$

$$I_{vas} = (\mathrm{Max}_{i=1...12}\{\gamma^2_{L_i}(S_2)\} \geq 1). \quad (7)$$

The alternating filter consists of the operations: a linear opening by reconstruction of size 15 (Eq. (5)), a linear closing by reconstruction of size 15 (Eq. (6)) and, finally, a linear opening of size 29 (Eq. (7)). This last operation removes bright or dark thin irregular zones [26] in the final stage of the filter.

2.3. Candidates Detection

After vessel segmentation, the image I_{lesion} which contains mainly non-elongated structures such as MAs is obtained by:

$$I_{lesion} = I_{sc} - I_{vas}. \quad (8)$$

The step related to candidate extraction starts at enhancing the contrast between background and MAs in I_{lesion}. At first, we apply a matched filter as a 2-D Gaussian with $\sigma = 1$ and size of 11 x 11 pixels, resulting in image I_{filt}. Next, a threshold is applied to I_{filt} to generate a binary image I_{bin}. The threshold used was fixed at a certain level above the modal value of the image histogram. From the experimental results, we set the threshold as a gray level equal to 7. It depends on the set of test images. After applying the matched filter, regardless the set of images used, the gray levels of the candidate MAs are close to the background. We have observed that when we set the threshold in a value less than 7 the amount of segmented candidates was reduced. Differently, a higher value tended to segment noisy data as candidates.

The extracted binary objects in I_{bin} do not represent the real forms of the pathologies found in I_{org}. Thus, a region growing procedure was used to grow back the original pathologies. The darkest pixel under each of the binary objects serves as the starting point.

The estimated background image I_{bg} obtained in the preprocessing step can be used to find the threshold for the region growing procedure as follows:

$$t = i_{seed} - x(i_{seed} - i_{bg}), \quad (9)$$

where i_{seed} is the intensity at the starting position, i.e., the pixel under the binary object with the lowest gray value. Then, i_{bg} is the intensity of the same pixel in the background image and $x \in [0, 1]$. Similarly to Frame *et al.*[5] and Spencer *et al.* [23], we set $x = 0,5$ in our algorithm. The region growing algorithm starts in the seed pixel and stops when no more connected pixels below the threshold can be found. The grown objects, of each image, form the final set of candidates.

2.4. Feature Extraction

Representative feature extraction of the detected candidate MAs constitute one of the most important task in the automatic MAs characterization scheme.

The features listed in Table 1 were presented by Spencer et al. [23] and they provide us a preliminary study of MAs classification. In Table 1, C corresponds to the number of pixels of each candidate MA, f_i is the i^{th} pixel, in gray levels, belonging to the green-plane of the original color image, after shade correction.

In addition to the features listed in Table 1, Cree *et al.* [2] suggested others to provide more consistency in the intensity measurements of images with quality and contrast variable. These features, listed in Eq. (10) to Eq. (13), use parameters as the mean $\bar{x}$ and the standard deviation σ, from

Features	Equations
Area	$a = \sum_{i \in C} 1$
Perimeter	p
Circularity	$c = \frac{p^2}{4\pi a}$
Intensity 1	$i_i = \sum_{i \in C} f_i$
Intensity 2	$i = \sum_{i \in C} s_i$
Mean-intensity 1	$m_i = \frac{i_i}{a}$
Mean-intensity 2	$m = \frac{i}{a}$

Table 1. Measured features from each candidate MA.

the difference, in gray levels, between the image I_{green} and the image I_{sc}.

$$I_i = \frac{1}{\sigma}(i_i - \bar{x}) \tag{10}$$

$$I = \frac{1}{\sigma} i \tag{11}$$

$$M_i = \frac{1}{\sigma}(m_i - \bar{x}) \tag{12}$$

$$M = \frac{1}{\sigma} m \tag{13}$$

2.5. Neural Network Classification

The choice of learning algorithm, network topology and input signal presentations are important factors in the learning performance [8]. In order to estimate the classification performance from the feature data set of candidate MAs, we used tree layers MLP (Multilayer Perceptron) neural networks with log-Sigmoid transfer functions in the hidden layer (5 neurons) and linear function in the output layer. This topology has also shown its merits in other pattern recognition applications [13, 19].

A backpropagation (BP) algorithm was employed to train the neural network using Levenberg-Marquardt (LM), a second-order nonlinear optimization technique. It was chosen from others BP training algorithms available, as the gradient descent with momentum, because its faster weights and biases update through an approximation to the Hessian matrix [7]. The experiments achieved satisfactory generalization at less than 10 epochs with learning rate 0.01. The accuracy of the networks are evaluated for each epoch in the training through mean squared error (MSE).

In supervised learning, generalization is the ability to provide accurate output values for input variables that have not been seen by the network [8]. Lack of generalization is caused by overfitting, where the network has memorized the training examples, but it has not learned to generalize to new samples [11]. A common technique to circumvent overfitting is based on an early stopping criterion to improve the network training speed and efficiency [8].

Thus, the training is stopped when the validation error begins to increase, and the weights and biases will then be derived at the minimum error.

The neural network estimates the candidates class from various input images, each described by a feature vector. This set of attributes have different magnitudes which may not reflect their relative importance in determining the required output class [11]. Therefore, the input vectors $\mathbf{x}$ and targets should be normalized to improve the performance of the network. Here, the means $\bar{\mathbf{x}}$ and standard deviations σ of the data sets were computed for scaling the inputs and targets. The normalization was applied as follows:

$$\mathbf{x}' = \frac{\mathbf{x} - \bar{\mathbf{x}}}{\sigma}. \tag{14}$$

Prediction of success of the neural network is assessed by Receiver Operating Characteristic (ROC) analysis. In its tabular form the ROC analysis display true and false positive and negative totals and sensitivity and specificity for each listed cutoff value between 0 and 1. To analyze the output data that are obtained from the application, sensitivity (true positive ratio), and specificity (true negative ratio) are calculated by using confusion matrix. Sensitivity value (same positive result with the manual diagnosis for MAs) is calculated by dividing the total of true positive candidates TP to total N of candidates. The specificity value (same diagnosis with the manual diagnosis for non-MAs) is calculated by dividing the total of negative candidates TN to total candidate numbers N. The area under curve (AUC) summarizes the accuracy of the classifier. The classifier average performance is better as the AUC is close to 1.

3. Results

The segmentation process was tested and evaluated on DRIVE database [24], a publicly available database of colored images. The DRIVE database consists of 40 images (seven of which present pathology), along with manual segmentations of the vessels. The images are captured in digital form from a Canon CR5 nonmydriatic 3CCD camera at 45 field of view (FOV). The images are of size 768x584 pixels, eight bits per color channel and have a FOV of approximately 540 pixels in diameter. The images are in compressed JPEG format, which is unfortunate for image processing but is commonly used in screening practice [21]. Figure 2(a) shows a retinal image (in the green band) provided for test in DRIVE database.

Using the methodology explained in Section 2, 25 feature vectors were extracted from the DRIVE images. MAs commonly appear as small dark nonelongated structures close to thinner blood vessels. Thus, the 25 samples were manually classified into 11 true candidate MAs and 14 false candidate MAs. Figure 2(b) shows the segmentation result of the image in Figure 2(a) with one true MA detected and highlighted in white. Figure 2(c) shows this MA in details.

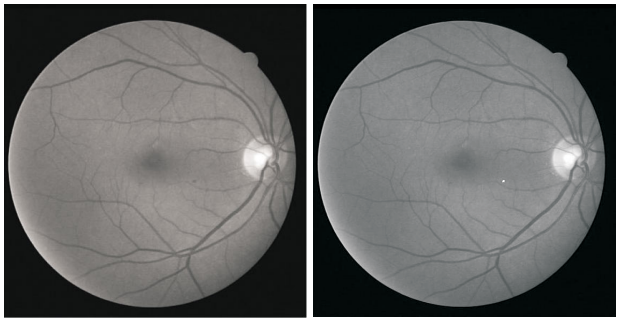

(a) An example of green band retinal image from DRIVE database.

(b) Full image with MA near the center.

(c) MA detail

Figure 2. Candidates detection on a retinal image.

Performing the neural network classification from the feature data set leads to 84% correct candidate characterization reaching satisfactory generalization on the average. To train the MLP classifier 70% of the feature vectors were randomly draw from the data set. The remainder 30% were used in the training stop criteria. As the number of samples is very small, all 25 feature vectors were used to assess the classifier performance. Table 2 shows confusion matrix and the true positive (TP=10) and true negative (TN=11) numbers obtained through MLP classifier where prediction fits real class. Although high false positive number (FP=3) which leads to false diabetic diagnosis, most important is the false negative number (FN=1) because it shows the system weakness in real diabetics retinopathy diagnosis is lower than 10%. As illustrated by the ROC curve in Figure 3 the classifier architecture has high sensitivity (TP ratio = 0.9091) and specificity (TN ratio = 0.7857) with value 0.9643 for the area under curve (AUC).

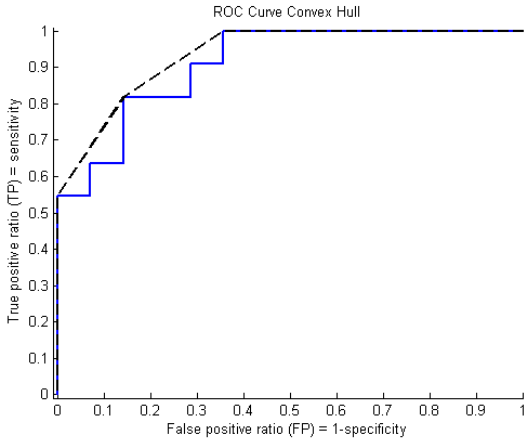

Figure 3. ROC curve of MLP neural network

Prediction/Real Class	MA	non-MA
MA	10	3
non-MA	1	11

Table 2. Test results of MLP Neural Network

4. Conclusion

We have developed a prototype system for candidate MAs detection in color fundus images with the goal of providing a suitable tool for diabetic retinopathy diabetic screening. This study has presented a methodology to vessels segmentation and MAs detection and characterization. Using it we are able to detect 100% of any candidate MAs.

A neural network was trained by the candidates feature set obtained from the segmented retinal digital image. The aim of this classification system is to test the performance of the feature sets. The testing performance is found to be satisfactory as 84% of the candidate MAs were correctly classified. Indeed, further work is necessary to achieve more reliable results in MAs characterization and, thus improve the diagnosis. The use of neural networks committees and feature combination has shown its merits in [18, 19]. Further development will assembled other modules into a system to establish medical diagnosis rapidly and accurately.

Acknowledgments

The authors are grateful to CNPq for financial support under grant No. 485070/2006-5.

References

[1] A. Bosco, A. C. Lerário, D. Soriano, R. F. dos Santos, P. Massote, D. Galvão, A. Cristina, S. Purish, and A. Rodrigues. Retinopatia diabética. *Arq Bras Endocrinol Metab*, 49(2):217–226, April 2005.

[2] M. J. Cree, J. A. Olson, K. C. McHardy, J. V. Forrester, and P. F. Sharp. Automated microaneurysm detection. In *International Conference on Image Processing*, volume 3, pages 699–702, Lausanne, September 1996.

[3] B. Fang, W. Hsu, and M. L. Lee. Reconstruction of vascular structures in retinal images. *International Conference on Image Processing*, 2:157–160, September 2003.

[4] A. D. Fleming, S. Philip, K. A. Goatman, J. A. Olson, and P. F. Sharp. Automated microaneurysm detection using local contrast normalization and local vessel detection. *IEEE Transactions on Medical Imaging*, 5(9):1223–1232, September 2006.

[5] A. J. Frame, P. E. Undrill, M. J. Cree, J. A. Olson, K. C. McHardy, P. F. Sharp, and J. Forrester. A comparison of computer based classification methods applied to the detection of microaneurysms in ophthalmic fluorescein angiograms. *Computers in Biology and Medicine*, 28:225–238, May 1998.

[6] F. D. Frate, A. Petrocchi, J. Lichtenegger, and G. Calabresi. Neural networks for oil spill detection using ERS-SAR data. *IEEE Transactions on Geoscience and Remote Sensing*, 38(5):2282–2287, September 2000.

[7] M.-H. Fun and M. T. Hagan. Levenberg-marquardt training for modular networks. *IEEE International Conference on Neural Networks*, 1:468–473, June 1996.

[8] S. Haykin. *Redes Neurais, princípios e prática*. Bookman, Porto Alegre, 2 edition, 2001.

[9] A. Hoover, V. Kouznetsova, and M. Goldbaum. Locating blood vessels in retinal images by piecewise threshold probing of a matched filter response. *IEEE Transactions on Medical Imaging*, 19(3):203–210, March 2000.

[10] Y. L. Huang and D. R. Chen. Watershed segmentation for breast tumor in 2-d sonography. *Ultrasound in Medicine and Biology*, 30(5):625–632, May 2004.

[11] A. K. Jain, R. P. Duin, and J. Mao. Statistical pattern recognition: a review. *IEEE Transactions on Pattern Analysis and Machine Intelligence*, 22(1):4–37, January 2000.

[12] H. J. Jelinek, M. J. Cree, D. Worsley, A. Luckie, and P. Nixon. An automated microaneurysm detector as a tool for identification of diabetic retinopathy in rural optometric practice. *Clinical and Experimental Optometry*, 89(5):299–305, September 2006.

[13] D. F. A. Lopes, G. L. B. Ramalho, F. N. S. de Medeiros, R. C. S. Costa, and R. T. S. Araújo. Combining features to improve oil spill classification in SAR images. *SSPR 2006. Lecture Notes in Computer Science, Berlim*, 4109:928–936, August 2006.

[14] A. M. Mendonça, A. C. Campilho, and J. M. R. Nunes. Automatic segmentation of microaneurysms in retinal angiograms of diabetic patients. In *International Conference on Image Analysis and Processing (ICIAP)*, pages 728–733, Veneza, 1999.

[15] M. Niemeijer, B. van Ginneken, J. Staal, M. S. A. Suttorp-Schulten, and M. D. Abràmoff. Automatic detection of red lesions in digital color fundus photographs. *IEEE Transctions on Medical Imaging*, 24(5):584–592, May 2005.

[16] N. Patton, T. M. Aslam, T. MacGillivray, I. J. Deary, B. Dhillon, R. H. Eikelboom, K. Yogesan, and I. J. Constable. Retinal image analysis: Concepts, applications and potencial. *Progress in Retinal and Eye Research*, 25:99–127, 2006.

[17] S. J. Preece and E. Claridge. Monte Carlo Modelling of the spectral reflectance of the human eye. *Physics in Medicine and Biology*, 47:2863–2877, July 2002.

[18] G. L. B. Ramalho and F. N. S. de Medeiros. Using boosting to improve oil spill detection in SAR images. In *18th International Conference on Pattern Recognition (ICPR 2006)*, volume 2, pages 1066–1069, Hong-Kong, August 2006.

[19] G. L. B. Ramalho and F. N. S. de Medeiros. Improving reliability of oil spill detection systems using boosting for high-level feature selection. *ICIAR2007. Lecture Notes in Computer Science*, 4633:1172–1181, August 2007.

[20] M. D. U. V. Removal and C. H. Transform. Sherif abdelazeem. In *9th National Radio Science Conference*, pages 421–426, Alexandria, March 2002.

[21] J. V. B. Soares, J. J. G. Leandro, R. M. C. Jr., H. F. Jelinek, and M. J. Cree. Retinal vessel segmentation using the 2-D gabor wavelet and supervised classification. *IEEE Transactions on Medical Imaging*, 25(9):1214–1222, September 2006.

[22] P. Soille. *Morphological Image Analysis*. Springer, second edition, 2003.

[23] T. Spencer, J. A. Olson, K. C. McHardy, P. F. Sharp, and J. V. Forrester. An image-processing strategy for the segmentation and quantification of microaneurysms in fluorescein angiograms of the ocular fundus. *Computers and Biomedical Research*, 29(21):284–302, May 1996.

[24] J. J. Staal, M. D. Abràmoff, M. Niemeijer, M. A. Viergever, and B. van Ginneken. Ridge based vessel segmentation in color images of the retina. *IEEE Transactions on Medical Imaging*, 23(4):501–509, April 2004.

[25] L. Streeter and M. J. Cree. Microaneurysm detection in colour fundus image. In *Image and Vision Computing NZ*, pages 280–285, Palmerston North, November 2003.

[26] F. Zana and J.-C. Klein. Segmentation of vessel-like patterns using mathematical morphology and curvature evaluation. *IEEE Transactions on Image Processing*, 10(7):1010–1019, July 2001.